



Research Article

Research on Oscillating Characteristics of the Shear Layer on the Ship Bottom with a Moonpool under the Action of the Current and Wave

X. H. Huang ¹, X. L. Yao,¹ Z. Y. Shi,² and W. Xiao ¹

¹College of Shipbuilding Engineering, Harbin Engineering University, Harbin 150001, China

²Marine Design & Research Institute of China, Shanghai 200003, China

Correspondence should be addressed to W. Xiao; wxiao@hrbeu.edu.cn

Received 7 December 2020; Revised 21 January 2021; Accepted 12 March 2021; Published 24 March 2021

Academic Editor: Fangqing Wen

Copyright © 2021 X. H. Huang et al. This is an open access article distributed under the Creative Commons Attribution License, which permits unrestricted use, distribution, and reproduction in any medium, provided the original work is properly cited.

For some research vessels, a sonar is installed in the moonpool, and some acoustic detection equipment are installed on the ship bottom behind the moonpool, which helps to avoid the impact of the high-speed flow. The moonpool causes the ship bottom discontinued, forming a particular shear layer oscillation. The shear layer oscillation affects the bubble generation and motion in and behind the moonpool. The sonar and acoustic equipment will malfunction when surrounded by many bubbles. However, there is almost no research on the shear layer oscillation near the moonpool. So, in this paper, by measuring the pressure near the moonpool and monitoring the fluid motion in the moonpool and bubbles' distribution along the ship bottom, the shear layer oscillation near the moonpool is studied experimentally under the action of the incident current and wave. Furthermore, the effects of the sonar and the moonpool shape are investigated. It can be seen that the shear layer oscillation excites the fluid motion in the moonpool. The sonar forms a complicated boundary in the moonpool, resulting in the increase in the frequency of the shear layer oscillation. The shear layer propagates along the ship bottom in the form of the ship bottom wave. Clarifying the oscillating characteristics of the shear layer along the ship bottom with a moonpool is conducive to the design of moonpools in the research ships, and the detection instruments are arranged in the right place along the ship bottom, so as to make sure the detection instruments work properly and detect the marine environment more accurately.

1. Introduction

Some research vessels are equipped with sonars and acoustic detection instruments to detect the marine environment. The sonar is installed in the moonpool to avoid the impact of high-speed fluid. The acoustic detection instruments used in conjunction with the sonar are arranged on the ship bottom behind the moonpool [1–4]. The moonpool causes the ship bottom discontinued. The sonar is of variable cross sections, which forms a complex boundary in the moonpool. A particular shear layer oscillation is formed near the moonpool. The shear layer oscillation affects the bubble generation and motion in and behind the moonpool. On the one hand, bubbles gather around the sonar; on the other hand, the bubbles expel from the moonpool, forming the bubble layer under the acoustic detection instrument. Under

the interference of bubbles, sonar and detection instruments work abnormally. Both bubble generation and motion are closely related to the shear layer oscillation.

There are two fluid motions in the moonpool, which are vertical piston motion and horizontal sloshing motion [5–7]. The fluid motion amplitude became intense coupling with some adverse effects in the resonant case. The adverse effects were the increase in resistance, increase in structural motion, green water, and so on [8–13]. To reduce the adverse effects, the damping devices were researched [14–18].

Most objects of the research studies on the shear layer oscillation were aerodynamic cavity instead of the moonpool [19–23]. The shear oscillation was studied by visual methods such as laser Doppler velocity measurement (LDA) and particle image velocimetry (PIV) [24–26]. The shear layer oscillation often occurred in an unbounded jet, a cavity flow,

a bluff body flow, and so on [27, 28]. The studies of shear layer oscillation were about flow separation and feedback disturbance [29, 30]. There were many disturbances in the shear layer oscillation. When the amplitude of the disturbance increased, it caused the instability of the oscillation. And the disturbance was enhanced by the pressure wave, which was formed on the impact wall [31–34].

As mentioned above, it can be found that most of the research studies on shear layer oscillations are about the open cavity flow or the jet. However, there is not too much research about the shear layer oscillation near the moonpool. To know the motion mechanism of the fluid and bubbles near the moonpool, there is a critical need to study the shear layer oscillation near the moonpool. In this paper, under the action of the incident current and wave, the shear layer oscillation near the moonpool is studied experimentally. By quantizing and analyzing the pressure near the moonpool and monitoring the fluid motion in the moonpool, the effects of the sonar and the moonpool shape on the shear layer oscillation are investigated. Furthermore, by monitoring the bubbles' distribution along the ship bottom, the propagation of the shear layer along the ship bottom is researched.

The rest of this paper is organized as follows. In Section 2, we present the experiment setup and data processing method. Under the action of the incident current, the influence of the sonar, the flow speed, and the moonpool shape on the fluid motion and the shear layer oscillation is investigated in Section 3. In Section 4, the fluid motion and the shear layer oscillation in the moonpool under the combined action of the wave and current are researched. The ship bottom wave, which is a flowing form of the free shear layer oscillation along the ship bottom, is analyzed in Section 5. Finally, we conclude the paper in Section 6.

2. Experiment Setup and Data Processing Method

2.1. Experiment Setup. The experiment is carried out in a towing tank, which is 108 m long, 7 m wide, and 4.5 m deep. The wave maker is located at the front of the towing tank. To illustrate the experiment setup, Figure 1 gives the experiment layout. As shown in Figure 1, the ship model and the trailer are connected by a tow bar. The drag speed is between 0.1 m/s and 6.5 m/s. The motion accuracy of the trailer is 0.1%. To photograph the fluid motion in the moonpool, the back wall of the moonpool is transparent. A LED lamp and high-speed camera are used to monitor the fluid motion in the moonpool. The ship model is 4 m long, 1.357 m wide, and 0.357 m in draught. To study the influence of the moonpool shape on the shear layer oscillation, a square moonpool and a rectangular moonpool are set up in this paper. The square moonpool is 0.257 m wide and 0.357 m in draught. The rectangular moonpool is 0.257 m long, 0.2 m wide, and 0.357 m in draught. The bottom edge of the moonpool near the bow is the leading edge. The bottom edge of the moonpool near the stern is the trailing edge. The sonar is of variable cross sections. To measure bubble width and height at different transverse sections of the ship, the PIV is arranged on the side of the ship model. The traditional tracer particles will be suspended in water for a long time, and the bubbles will

automatically dissipate in water. Therefore, bubbles are chosen to replace the traditional tracer particles as a tracer to meet the requirements of multiple tests in a short time. The change in the distribution of bubbles on the cross section reflects the influence of the shear layer oscillation. To ensure a sufficient amount of bubbles, air is ventilated into water through the vent to generate artificial bubbles. The vent is located at the leading edge. The ventilation volume is set to 100 L/min.

To measure the fluid pressure change near the moonpool, seven pressure sensors are arranged along the ship bottom. The midpoint of the leading edge is set as the original coordinate. The forward direction of the stern to the bow is the positive direction of the X -axis; the forward direction of the ship middle to starboard is the positive direction of the Y -axis; and the vertical upward direction is the positive direction of the Z -axis. The coordinates of the pressure sensor are shown in Table 1. Sensor 1 is installed below the free surface. Sensors 2–4 are installed at the moonpool bottom. Sensors 5–7 are installed along the ship bottom behind the moonpool.

Twenty-one test cases are set in the paper. The details of the test cases are given in Table 2. The setting of the test cases includes the following influencing factors, such as the moonpool shape, the sonar, the flow speed, and the incident wave.

We considered the uncertainty level of the experiment. According to the tank dimensions, we reasonably design the ship model. To obtain accurate data, the high-precision trailers, PIV, high-speed cameras, and pressure sensors are selected. The experimental data are verified with the experimental phenomena mutually. Bubbles are used as tracer particles to meet the requirements of multiple tests in a short time. One case is repeated several times, and the experimental results are consistent with each other, indicating that the experimental accuracy is good.

2.2. Data Processing Method. In this experiment, the pressure data are measured by the pressure sensors. The pressure data are nonstationary and random. There are some signals with multiple frequencies in the original pressure signal. The stationary Gaussian signal can be transformed using the Fourier method. The nonstationary and random signal can be transformed using the short-time Fourier transform (STFT), wavelet transform, and empirical mode decomposition (EMD). EMD was proposed by N. E. Huang and others at the National Aeronautics and Space Administration. In this paper, to obtain the intrinsic mode functions (IMFs) representing different oscillation modes, the empirical modal decomposition (EMD) method is used to decompose the original pressure signal. The signal processing steps are as follows. First, as shown in equation (1), the mean value of the signal is calculated:

$$m_1(t) = \frac{e_{\text{up}}(t) + e_{\text{down}}(t)}{2}, \quad (1)$$

where $m_1(t)$ is the mean value of the original signal; $e_{\text{up}}(t)$ is the max value; and $e_{\text{down}}(t)$ is the min value.

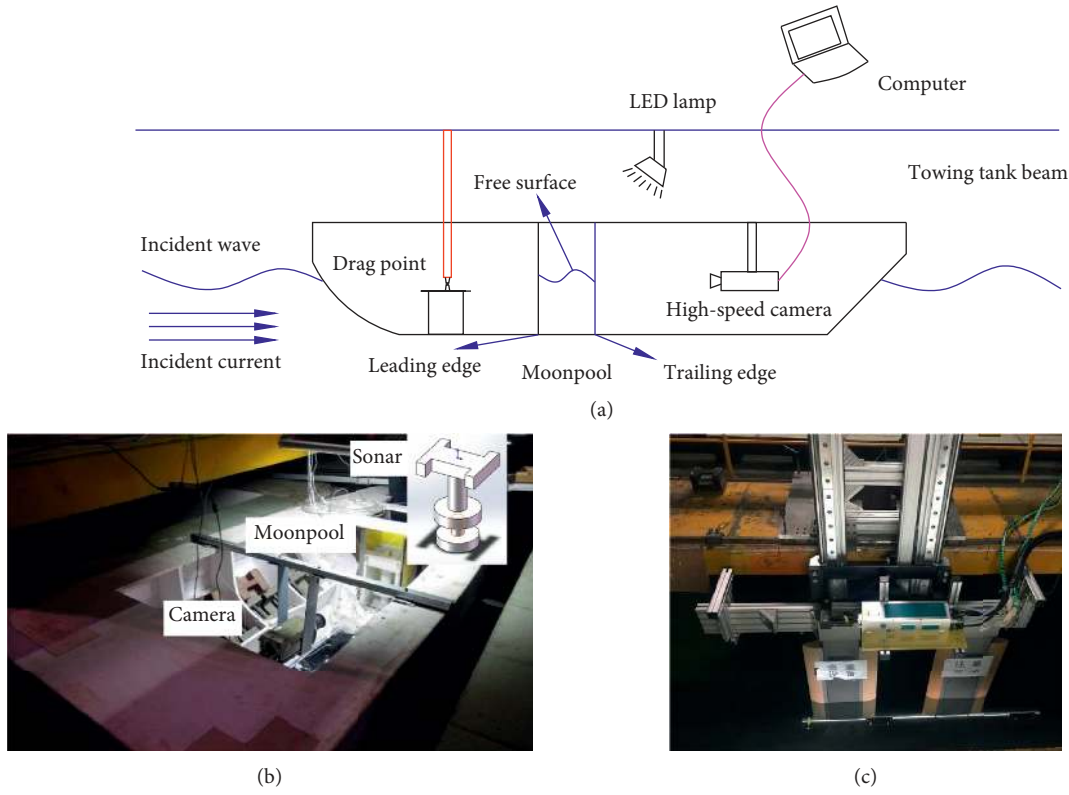


FIGURE 1: Experiment layout. (a) Schematic diagram of the experiment setup. (b) Ship model. (c) PIV.

The original signal is subtracted from the average value to obtain $h_1(t)$. After repeating the above steps k times, the obtained signal meets the requirements of the eigenmode function.

$$\begin{aligned} h_1(t) &= x(t) - m_1(t) \\ h_2(t) &= h_1(t) - m_2(t) \\ &\vdots \\ h_k(t) &= h_{k-1}(t) - m_k(t), \end{aligned} \quad (2)$$

where $h_1(t)$, $h_2(t)$, $h_{k-1}(t)$, and $h_k(t)$ are the signals obtained after the first, second, $k-1$ -th, and k -th processing, respectively, $x(t)$ is the original signal, and $m_2(t)$ and $m_k(t)$ are the mean values of the signals obtained in the first and k -th processing, respectively.

Different eigenmode functions are separated from the original signal through different calculations and cycles of equations (1) and (2).

$$\begin{aligned} r_1(t) &= x(t) - c_1(t) \\ r_2(t) &= r_1(t) - c_2(t) \\ &\vdots \\ r_N(t) &= r_{N-1}(t) - c_N(t), \end{aligned} \quad (3)$$

where $c_1(t)$ is $h_k(t)$ obtained from the first loop; $c_2(t)$ and $c_N(t)$ are obtained from the second and N -th loop; $r_1(t)$ is the remaining signal after subtracting the $c_1(t)$ signal from the original signal; $r_2(t)$ is the remaining signal after

subtracting the $c_2(t)$ signal from the $r_1(t)$ signal; $r_2(t)$ is the remaining signal after subtracting the $c_2(t)$ signal from the $r_1(t)$ signal; and $r_N(t)$ is the remaining signal after subtracting the $c_N(t)$ signal from the $r_{N-1}(t)$ signal.

Finally, the original signal $x(t)$ can be expressed as shown in the following equation:

$$x(t) = \sum_{i=1}^N c_i(t) + r(t). \quad (4)$$

To better illustrate the analysis process of the pressure signal, the pressure signals of sensor 2 and IMF are given in Figure 2. As shown in Figure 2, the original pressure signal is decomposed by the empirical modal method to obtain 10 IMFs. There are two high peaks that appear when t is 2.26 s and 6.87 s in the original pressure signal. They are due to the acceleration and deceleration of the trailer. Therefore, IMFs 1~3 are the interference signal in the test.

To illustrate the information contained in the IMF, the spectrum analysis maps (SAM) for IMFs 1~10 of sensor 2 are given in Figure 3. As shown in Figures 3(b) and 3(c), the frequency peak of SAM 3 is similar to that of SAM 4. So, IMFs 1~4 should be eliminated. The piston resonance motion in the moonpool occurs when the frequency of the shear layer oscillation is close to the natural frequency of the piston motion in the moonpool. The frequency of the shear layer oscillation can be estimated by calculating the natural frequency of the piston motion in the moonpool. A piston natural frequency formula of the moonpool was obtained in our previous paper [35]:

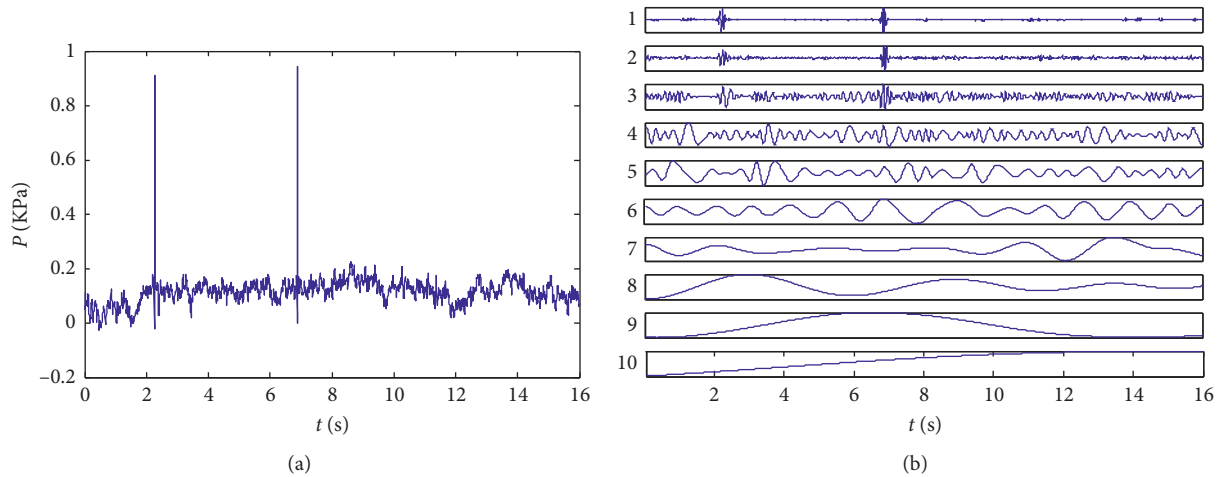
TABLE 1: Pressure sensors' coordinates.

No.	Coordinates
Sensor 1	(0, 0, 0.3)
Sensor 2	(0, 0, 0)
Sensor 3	(0.257, 0, 0)
Sensor 4	(0.257, 0.1, 0)
Sensor 5	(0.4, 0, 0)
Sensor 6	(0.86, 0, 0)
Sensor 7	(1.33, 0.075, 0)

TABLE 2: Test cases.

Model	Wave	Fr (Froude number)
Model 1: rectangular moonpool with a sonar	No wave	0.81, 1.07, 1.32, 1.58, 1.83
	Wave 1, wave 2, wave 3	1.83
Model 2: rectangular moonpool without a sonar	No wave	0.81, 1.07, 1.32, 1.58, 1.83
Model 3: square moonpool with a sonar	No wave	0.81, 1.07, 1.32, 1.58, 1.83
	Wave 1, wave 2, wave 3	1.83

Wave 1: $h = 0.03$ m, $\lambda = 0.39$ m, and $T = 0.5$ s; wave 2: $h = 0.03$ m, $\lambda = 1.56$ m, and $T = 1$ s; wave 3: $h = 0.03$ m, $\lambda = 6.25$ m, and $T = 2$ s (h is the wave height, λ is the wave length, and T is the wave period)

FIGURE 2: Original pressure signals of sensor 2 and IMF in the square moonpool with $Fr = 1.32$. (a) Original signal. (b) IMF.

$$f_0 = \frac{1}{2\pi} \sqrt{\frac{g}{d + (\pi L/8)}}, \quad (5)$$

where d is the draught of the moonpool and L is the length of the moonpool.

The calculated frequency of the piston motion in the moonpool is 0.74 Hz. The frequency peak of SAM 10 is 0.06248 Hz. SAM 10 with a low frequency is the accumulated error during the signal decomposition process. So, IMF 10 should be eliminated. The frequency peaks of SAMs 5~9 are given in Table 3. The oscillation frequency of the shear layer has not been confirmed until this time.

The shear layer flows from the leading edge to the stern and impacts on the trailing edge. Sensor 2 is located at the leading edge; sensor 3 is located at the trailing edge. Therefore, the oscillation frequencies of the shear layer at sensors 2 and 3 should be similar. The frequency peaks of SAMs 4~8 are given in Table 4.

Comparing the frequency peaks of the spectrum analysis maps in Tables 3 and 4, it can be found that there is a same value, which is 2.187 Hz. Therefore, 2.187 Hz is the frequency of the first-order shear layer oscillation with $Fr = 1.32$. Similarly, the frequency of the second-order shear layer oscillation is 3.311 Hz.

3. Under the Action of the Incident Current

3.1. Influence of the Sonar on the Fluid Motion and the Shear Layer Oscillation. To study the fluid motion in the moonpool without a sonar, Figure 4 gives the max fluid motion in the rectangle moonpool without a sonar at different speeds. As shown in Figures 4(a) and 4(b), when Fr is 0.81 and 1.07, the sailing speed and the motion amplitude of the free surface are relatively small. The free surface motion is caused by the motion of the ship hull. It shows that the shield effect of the moonpool is obvious.

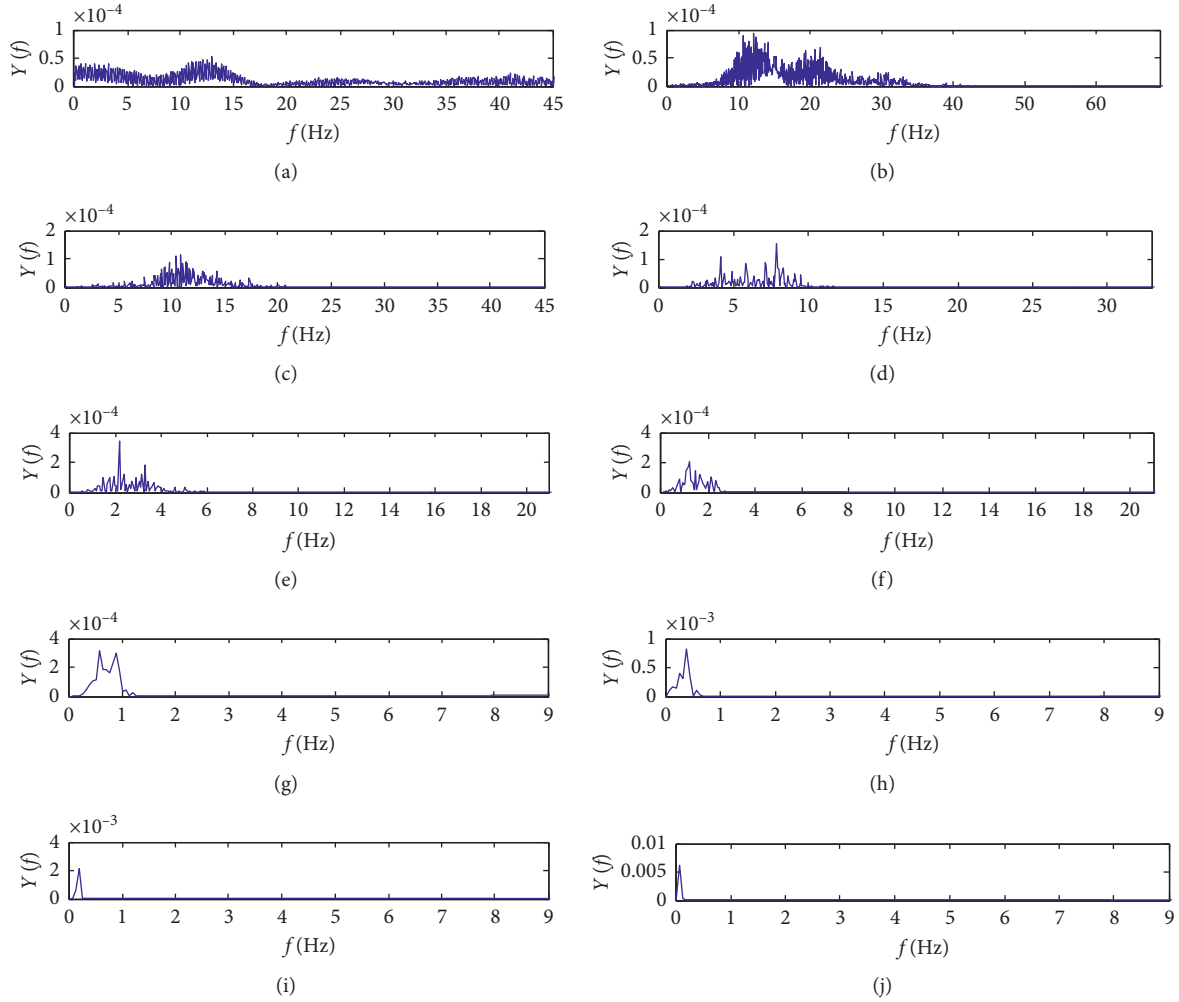


FIGURE 3: Spectrum analysis maps (SAM) for IMFs 1 ~ 10 of sensor 2 in the square moonpool with $Fr = 1.32$. (a) SAM 1 for IMF 1. (b) SAM 2 for IMF 2. (c) SAM 3 for IMF 3. (d) SAM 4 for IMF 4. (e) SAM 5 for IMF 5. (f) SAM 6 for IMF 6. (g) SAM 7 for IMF 7. (h) SAM 8 for IMF 8. (i) SAM 9 for IMF 9. (j) SAM 10 for IMF 10.

TABLE 3: Frequency peaks of SAMs 5~9 for sensor 2 in the square moonpool with $Fr = 1.32$.

SAM	5	6	7	8	9
Frequency peak (Hz)	2.187, 3.311	1.187	0.5623, 0.8747	0.3749	0.1874

TABLE 4: Frequency peaks of SAMs 4~8 at sensor 3 in the square moonpool with $Fr = 1.32$.

SAM	4	5	6	7	8
Frequency peak (Hz)	2.812, 3.311, 3.624	1.375, 1.624, 2.187	0.6873, 0.9997	0.3124	0.2499

As shown in Figure 4(c), when Fr is 1.32, the sloshing motion in the moonpool is obvious. As shown in Figure 4(d), the maximum amplitude of the sloshing motion in the moonpool is 4.5 cm when Fr is 1.58. As shown in Figure 4(e), when Fr is 1.83, the amplitude of the sloshing motion increases to 6.5 cm. As Fr increases, the amplitude of the fluid motion in the moonpool increases, and the fluid motion becomes more intense.

Based on the theory of the shear layer oscillation and the structure characteristics of the moonpool, the mechanism of

the shear layer oscillation in the moonpool is analyzed. To analyze the fluid motion near the moonpool more vividly, a schematic diagram of the fluid motion near the moonpool is given in Figure 5. As shown in Figure 5, a boundary layer with a velocity gradient is formed at the leading edge of the moonpool. The boundary layer leaves the interface, which forms a free shear layer. A large amount of fluid flows into the moonpool from the rear of the moonpool and flows forward in the moonpool, which forms an internal circulation. Some other fluids flow downstream in the form of a

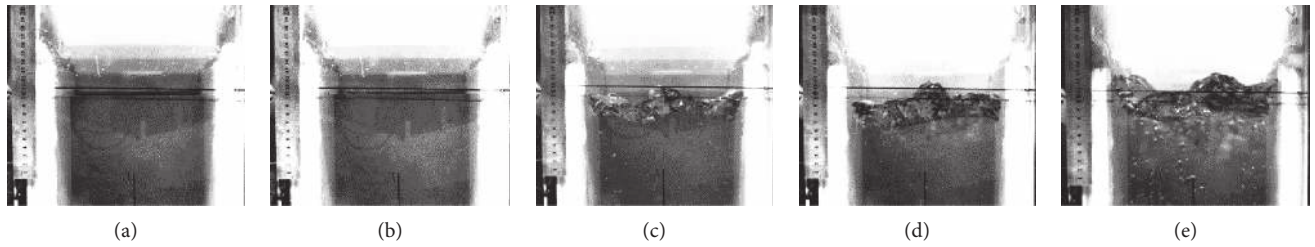


FIGURE 4: Max fluid motion at different speeds in the rectangle moonpool without a sonar. (a) $Fr = 0.81$. (b) $Fr = 1.07$. (c) $Fr = 1.32$. (d) $Fr = 1.58$. (e) $Fr = 1.83$.

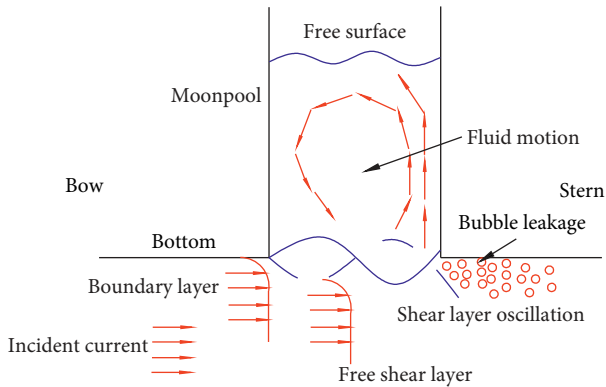


FIGURE 5: Fluid motion near the moonpool without a sonar.

free shear flow. It is consistent with results of the authors' previous research [35]. Many bubbles leak from the back of the moonpool. Due to the velocity gradient of the free shear layer, the instability of the shear layer oscillation is aggravated, and the fluid oscillation is amplified. The shear layer oscillation exacerbates the exchange of fluid inside and outside of the moonpool. Under the action of current, when the shear layer oscillation frequency is similar with the natural frequency of the piston motion or the sloshing motion, the resonance motion occurs in the moonpool.

Some fluid disturbances affect the free shear layer oscillation. The fluid disturbances are mainly of two types. One type is the hydrodynamic disturbance which is mainly the piston motion and the sloshing motion in the moonpool. The other type is pressure wave, which forms when the free shear layer oscillation impacts on the trailing edge of the moonpool. Ma (Mach number) is 0.002 in this paper, which is very small. The fluid flow speed is much less than the sound speed. Therefore, the influence of pressure wave on the free shear layer oscillation can be neglected. When the fluid disturbances promote the flow separation under the moonpool bottom, the shear layer oscillation is enhanced. A closed feedback loop is formed, and the free shear layer oscillation can be referred to as the self-sustained oscillation of the shear layer.

To better illustrate the influence of the sonar in the moonpool, Figure 6 gives the max fluid motion at different speeds in the rectangle moonpool with a sonar. As shown in Figure 6, the free surface is asymmetrical. The sloshing motion occurs in the moonpool. When Fr is 0.81, the amplitude of the free surface motion is only 0.9 cm. When Fr

is 1.83, the amplitude of the free surface motion is 3.5 cm. The amplitude of the sloshing motion increases as Fr increases. The greater Fr , the more intense the fluid motion in the moonpool.

The amplitude of the sloshing motion in the moonpool with a sonar is much smaller than that in the moonpool without a sonar. It is because that the sonar is of variable cross sections. The sonar takes up a lot of volume in the moonpool, reducing the space for the fluid motion in the moonpool. When the sonar is installed in the moonpool, the fluid near the sonar will flow around. The energy of the fluid motion in the moonpool is dissipated. In other words, the energy of the shear layer oscillation is dissipated.

Under the influence of the sonar in the moonpool, the mode of the fluid motion in the moonpool changes. To analyze the fluid motion near the moonpool with a sonar more vividly, a schematic diagram of the fluid motion near the moonpool with the sonar is given in Figure 7. As shown in Figure 7, under the action of the sonar, the large eddy with a low frequency is transformed into some small eddies. Therefore, the fluid motion in the moonpool changes. Under the action of the shear layer oscillation, bubbles leak from the moonpool.

3.2. Influence of Flow Speed on the Shear Layer Oscillation.

By the empirical modal decomposition method, the frequency of the shear layer oscillation near the moonpool at different flow speeds is analyzed. To better study the change law of the shear layer oscillation frequency, St (Strouhal number) of the shear layer oscillation is defined as

$$St = \frac{f \cdot L}{v}, \quad (6)$$

where f is the frequency of the shear layer oscillation; L is the length of the moonpool; and v is the flow speed.

To study the change law of St with Fr , Figure 8 gives the variation of St with Fr of sensor 2 in the square moonpool with a sonar. As shown in Figure 8, St changes little as Fr increases. According to the self-sustained oscillation theory of the shear layer, St increases with the increase of the flow speed under the feedback action of the pressure wave. If the feedback action is fluid dynamic, St does not change with the flow velocity. Therefore, the feedback action of the shear layer oscillation in the moonpool is fluid dynamic.

To verify the accuracy of the test, several tests are repeated four times. Figure 9 gives the variation of the first-

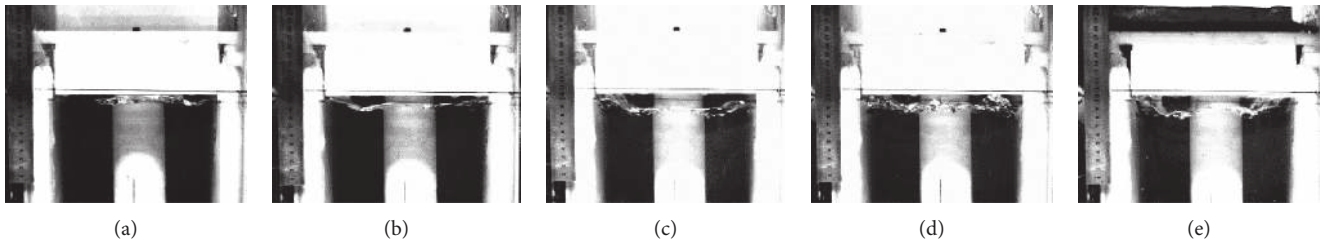


FIGURE 6: Max fluid motion at different speeds in the rectangle moonpool with a sonar. (a) $Fr = 0.81$. (b) $Fr = 1.07$. (c) $Fr = 1.32$. (d) $Fr = 1.58$. (e) $Fr = 1.83$.

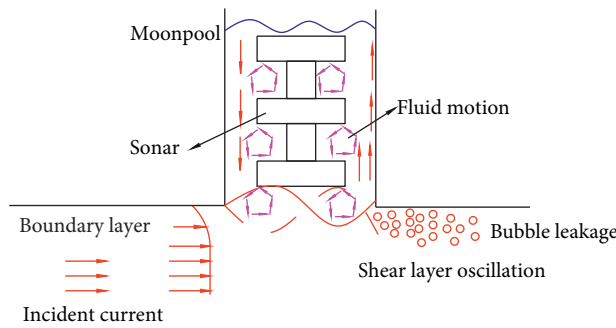


FIGURE 7: Fluid motion near the moonpool with a sonar.

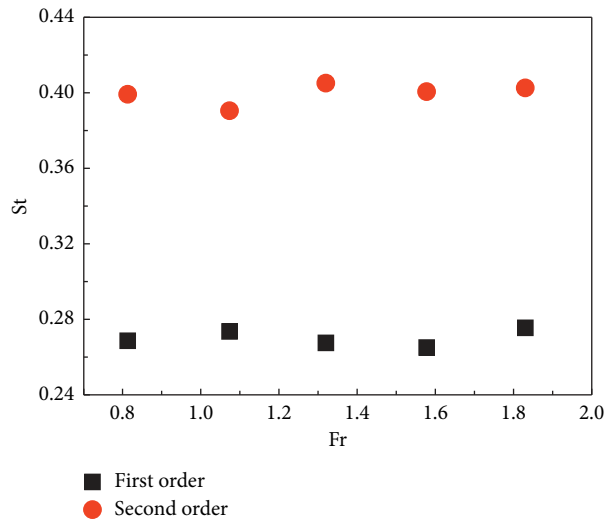


FIGURE 8: Variation of St with Fr of sensor 2 in the square moonpool with a sonar.

and second-order frequencies of the shear layer oscillation with Fr of sensor 2 in the square moonpool with a sonar. Results of Figure 9 are rather obvious; it would be enough to state that there is a good repeatability of the tests with a maximum error of 5%. It confirms the reliability of the test and data processing methods. However, when $Fr = 1.83$, the frequencies of the shear layer oscillation are not obtained in the fourth experiment.

To find out the reason that the fourth experiment results are different from the first three experiments, the fluid motion in the square moonpool with a sonar of the fourth experiment is given in Figure 10. As shown in Figure 10, the piston motion in

the moonpool is obvious. The period of the piston motion is approximately 1.29 s. A frequency peak of 0.777 Hz can be obtained from the data of sensor 2. Therefore, 0.777 Hz is the piston motion frequency. To verify the fluid motion form in the moonpool with $Fr = 1.83$, sixteen experiments are repeated. In the three tests with $Fr = 1.83$, the piston motion in the moonpool is obvious. In the other three experiments, the sloshing motion in the moonpool is obvious.

When the piston motion occurs in the moonpool, the shear layer oscillation is not captured by the pressure sensors. It indicates that the piston motion breaks the shear layer oscillation. During the trailer acceleration, the fluid in the moonpool

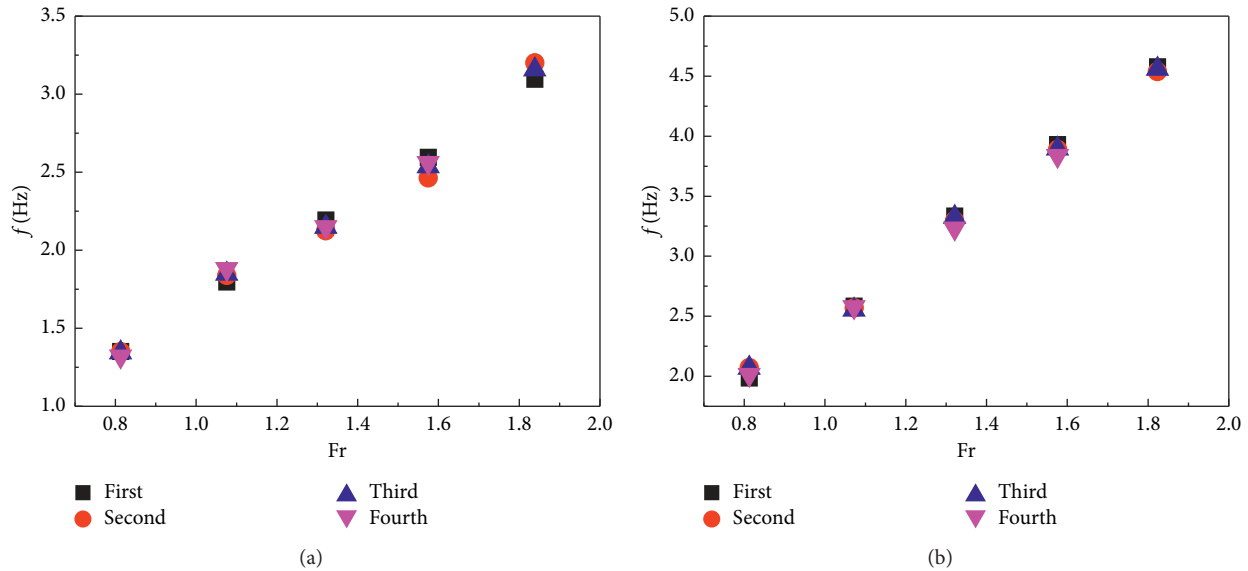


FIGURE 9: Variation of the first- and second-order frequencies of the shear layer oscillation with Fr of sensor 2 in the square moonpool with a sonar. (a) First order. (b) Second order.

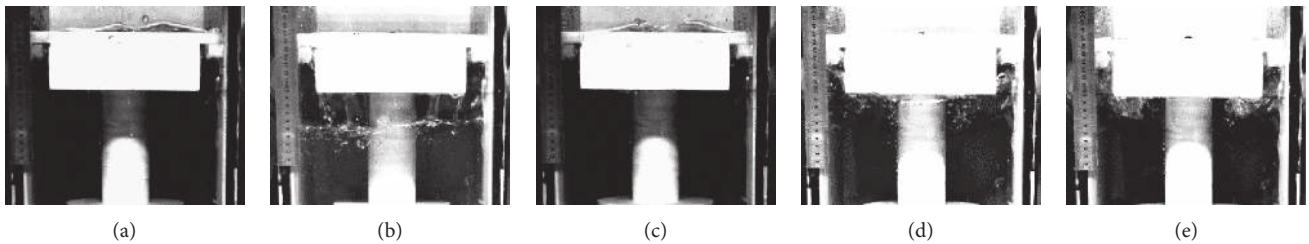


FIGURE 10: Fluid motion in the square moonpool with a sonar of the fourth experiment ($Fr = 1.83$). (a) $t = 10.10$ s. (b) $t = 10.74$ s. (c) $t = 11.39$ s. (d) $t = 12.30$ s. (e) $t = 12.94$ s.

leaves the equilibrium position. When the ship model is sailing, the motion velocity of fluid outside the moonpool is greater than that in the moonpool. Therefore, the pressure in the moonpool is greater than the pressure outside the moonpool. The fluid in the moonpool will flow out of the moonpool under the action of the pressure difference. The fluid inside and outside the moonpool communicates with each other and contacts with the air directly. The atmospheric pressure will cause the external fluid of the moonpool to flow into the moonpool again. Therefore, a one-dimensional vibration system is formed, which produces a phenomenon similar to Helmholtz resonance. The amplitude of such piston motion is much greater than that caused by the shear layer oscillation. This type of piston motion changes the hydrodynamic feedback model of the fluid oscillation in the moonpool. It also shows that the sloshing motion and the shear layer oscillation near the moonpool bottom influence each other. The fluid motion in the moonpool strengthens the separation of the free shear layer at the leading edge of the moonpool.

3.3. Influence of the Moonpool Shape on the Shear Layer Oscillation. To illustrate the influence of the moonpool shape on the shear layer oscillation, Figure 11 gives the

variation of St with Fr of sensor 2 in the rectangular moonpool with a sonar. As shown in Figure 11(a), St changes little as Fr increases. Compared with the result for the square moonpool in Figure 8, the change law of St with Fr for the square and rectangular moonpool with a sonar is similar. It indicates that the width is not an important feature scale for influencing the shear layer oscillation.

Sonar and the wall of the moonpool form complex boundary conditions for the fluid motion in the moonpool. To illustrate the influence of the complex boundary condition in the moonpool, Figure 11(b) gives the variation of St with Fr in the rectangular moonpool without a sonar. As shown in Figure 11(b), St changes little as Fr increases. Therefore, regardless of the change of the bottom size or the internal boundary in the moonpool, St changes little as Fr increases. It confirms that the feedback mode of the shear layer oscillation in the moonpool is fluid dynamic.

To illustrate the influence of the bottom shape and the boundary condition in the moonpool on the shear layer oscillation, Figure 12 gives the frequencies of the shear layer oscillation in different moonpools. As shown in Figure 12, the first and second frequencies of the shear layer oscillation in different moonpools increase as Fr increases. The first- and second-order frequencies for the square and rectangular

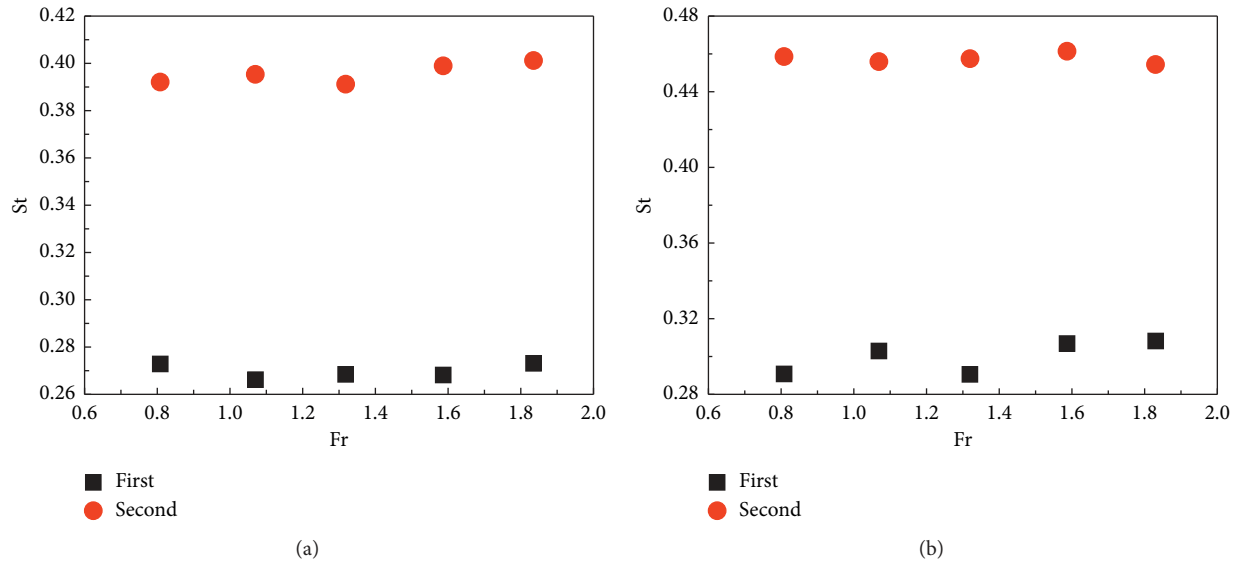


FIGURE 11: Variation of St with Fr of sensor 2 in the rectangular moonpool with a sonar. (a) With a sonar. (b) Without a sonar.

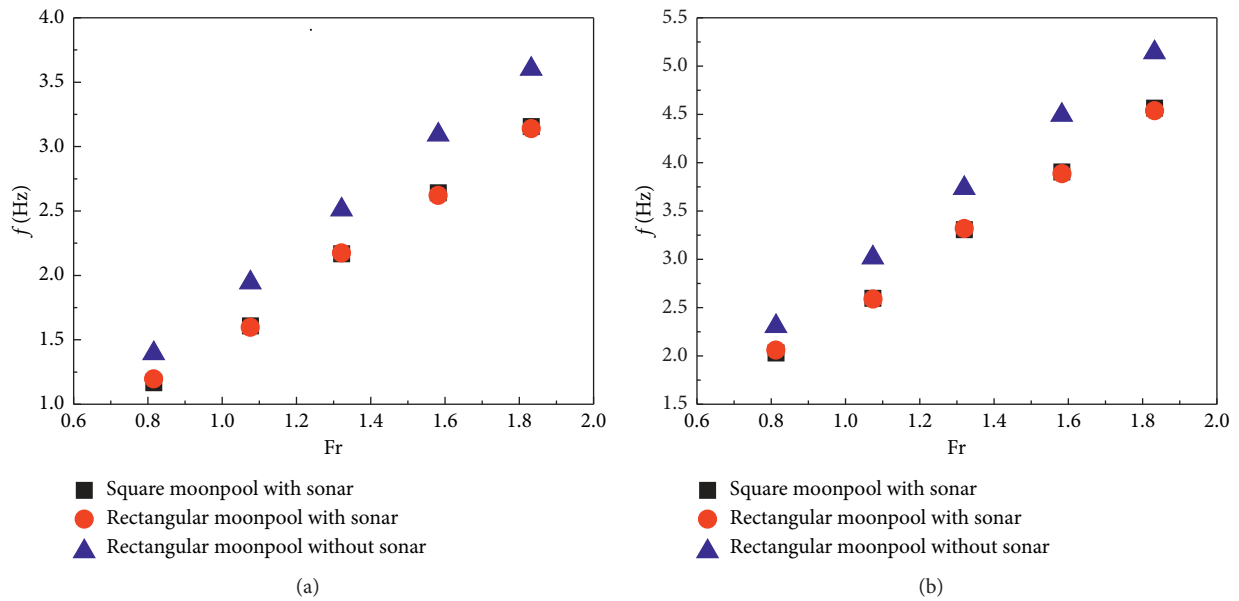


FIGURE 12: Frequencies of the shear layer oscillation in different moonpools. (a) First-order frequency. (b) Second-order frequency.

moonpools with sonars are similar. It indicates that the shear layer oscillation frequency is less affected by the width of the moonpool. When there is a sonar in the moonpool, the frequency of the shear layer oscillation increases.

The first-order frequency peak of the shear layer oscillation is larger than that of the second order and higher order. It shows that the energy of the shear layer oscillation is mainly concentrated on the first-order oscillation. When Fr is small, the frequency of the high-order shear layer oscillation is similar to the natural frequency of the fluid motion in the moonpool. However, at this time, the strength of the shear layer oscillation at a

low speed is relatively small. The amplitude of the free surface motion in the moonpool is relatively small. In other words, the excitation action of the high-order shear layer oscillation on the fluid motion in the moonpool is not obvious. Although the free surface oscillation is small, the pressure sensors can still capture the shear layer oscillation near the moonpool bottom. Therefore, the vortex motion in the moonpool should be the dominant factor of the fluid dynamics feedback.

Under the action of the incident current, the shear layer oscillation is the main excitation source for the fluid motion in the moonpool. The fluid motion in the moonpool is

forced. When the frequency of the shear layer oscillation is similar to the natural frequency of the fluid motion in the moonpool, the fluid motion in the moonpool will bring positive feedback to the shear layer oscillation. The resonance motion will occur in the moonpool. The frequency of the shear layer oscillation is directly related to the moonpool length, the boundary conditions in the moonpool, and the flow speed.

4. Under the Combined Action of the Incident Flow and Current

To illustrate the fluid motion in the moonpool under the combined action of the wave and current, Figure 13 gives the fluid motion in the square moonpool with a sonar under the combined action of the wave and current. As shown in Figure 13, the piston motion can be observed obviously between 19.75 s and 22.37 s. When t is 19.75 s, the fluid flows to the lowest point in the moonpool. Then, the free surface begins to rise. When t is 20.37 s, the fluid flows to the highest point in the moonpool.

As shown in Figure 13, when t is 14.93 s, there are sloshing motions in the moonpool. Therefore, the piston and the sloshing motion are coupled with each other in the moonpool under the combined action of the wave and the current. The fluid motion in the moonpool is mainly the sloshing motion under the action of the incident current. The action of the incident wave changes the fluid motion in the moonpool. Under the combined action of the wave and current, the period of the piston motion in the moonpool is about 1.26 s, which is similar to the natural oscillation period of the piston motion in the moonpool [35]. And some of them differ from the incident wave period. At the same time, under the combined action of the wave and the current, the biggest amplitude of the free surface motion in the moonpool is 7.5 cm, which is much larger than the one under the action of the incident current.

To illustrate the effect of waves on the fluid motion in the moonpool, Figure 14 gives the fluid motion in the moonpool under the action of different waves. As shown in Figure 14, under the action of wave 2, the sloshing motion, instead of the piston motion, occurs in the moonpool. Under the action of wave 3, the piston motion in the moonpool is obvious. The period of the piston motion is about 1.29 s, which is similar with the one under the action of wave 1. The amplitude of the free surface motion under the action of wave 1 is greater than that under the action of waves 2 and 3. This is because the wavelength of wave 1 is similar to the length of the moonpool. The standing wave occurs in the moonpool. For wave 1, two frequency peaks at the leading edge and the trailing edge are achieved, which are, respectively, 0.7918 Hz and 2.059 Hz. The frequency of the piston motion in the moonpool is about 0.8 Hz in the test. Thus, 0.7918 Hz is the frequency of the piston motion, and 2.059 Hz is the frequency of the incident wave.

Under the combined action of the wave and current, the self-sustained oscillation of the shear layer is not found. It is mainly because the incident waves change the

fluid motion in the moonpool, and the original shear layer oscillation is destroyed. The stable feedback of the shear layer oscillation cannot be formed. Under the action of the uniform flow, the excitation source of the fluid motion in the moonpool is the self-sustained oscillation of the shear layer. Under the combined action of the wave and current, the excitation source at this time is mainly the incident wave. The periodic rise and fall of the incident wave induces piston motion in the moonpool. When the incident wave transmits into the moonpool, the standing wave is formed in the moonpool, which induces the sloshing motion in the moonpool.

5. Ship Bottom Wave

To study the effect of the shear layer oscillation on the flow field along the ship bottom behind the moonpool, Figure 15 gives the distribution of bubbles on the transverse section at 1.07 m behind the square moonpool. As shown in Figure 15, the concentration, thickness, and width of bubbles change periodically. And the bubble behind the moonpool flows at a specific angle, which deviates from the longitudinal section in the center plane. From these various phenomena observed in the experiment, it can be found that there should be some kind of fluctuation along the ship bottom behind the moonpool. In the following paper, this fluctuation is called the ship bottom wave.

To study the formation cause of the ship bottom wave along the ship bottom behind the moonpool, a schematic diagram of the fluid motion near the moonpool is given in Figure 16. As shown in Figure 16, the shear layer oscillation separates at the moonpool bottom, forming the free shear layer oscillation. The fluid in the moonpool and outside the moonpool can be regarded as two kinds of fluids: the high-speed fluid outside the moonpool and the low-speed fluid in the moonpool. There is an interface between the two fluids. In our previous research, because the free surface sucks gas, bubbles are formed in the moonpool. The fluid density in the moonpool will change. This unstable flow phenomenon near the moonpool is similar to the Kelvin–Helmholtz instability. The interface between the two fluids changes constantly under the influence of the flow instability.

According to the theory of flow stability, in the parallel flow, the linear perturbation wave moves in the form of traveling waves. The motion direction of the traveling wave is consistent with that of the current. The ship bottom wave is a kind of traveling wave, which is due to the free shear layer flowing downstream. The bottom wave can be regarded as a kind of three-dimensional Tollmien–Schlichting wave (T-S wave). The distribution of the bubble layer in the width direction behind the moonpool should be affected by a diffusion effect of the T-S wave.

To illustrate the oscillation characteristic of the shear layer near the moonpool, Figure 17 gives the spectrum analysis maps for the shear layer oscillation at different points along the ship bottom with $Fr = 1.83$. As shown in Figure 17, the frequency peak of the shear layer oscillation at the trailing edge is much larger than that at the leading edge.

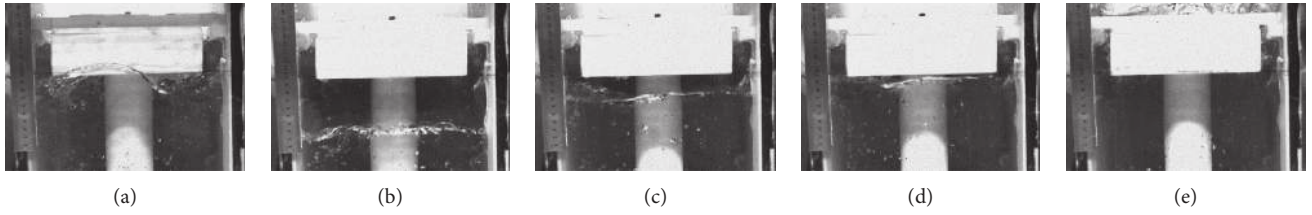


FIGURE 13: Fluid motion in the square moonpool with a sonar under the combined action of the wave ($h = 0.03$ m, $\lambda = 0.39$ m, and $T = 0.5$ s) and current ($Fr = 1.83$). (a) $t = 14.93$ s. (b) $t = 19.75$ s. (c) $t = 20.01$ s. (d) $t = 20.04$ s. (e) $t = 20.37$ s.

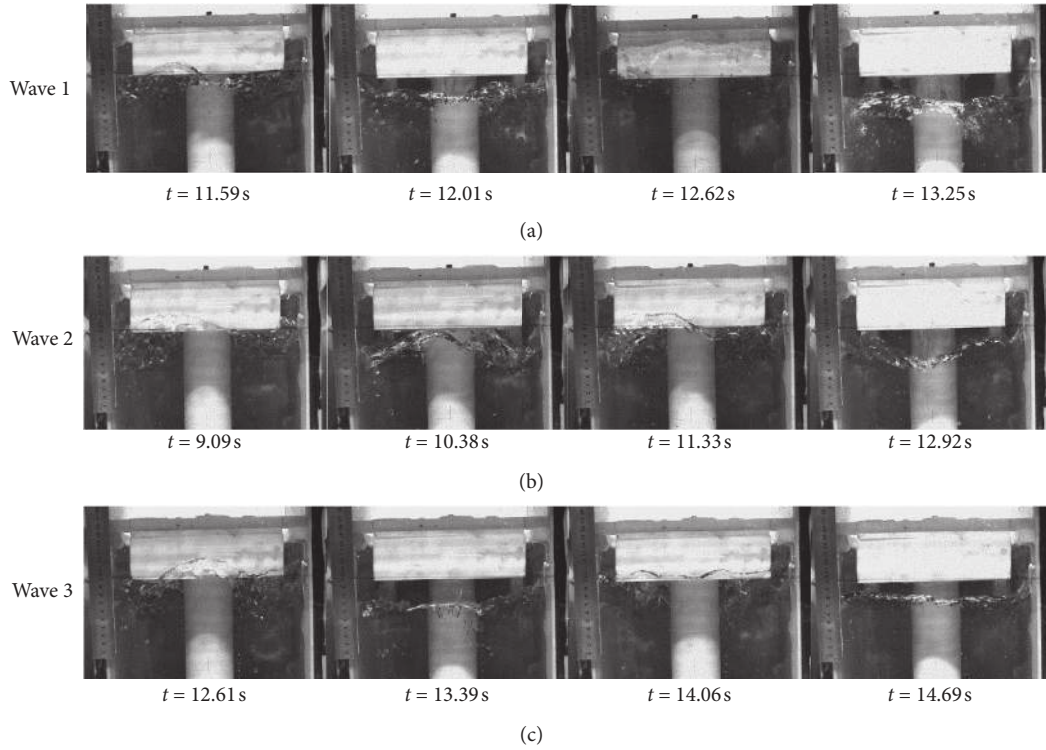


FIGURE 14: Fluid motion in the square moonpool with a sonar under the action of different waves (wave 1: $h = 0.03$ m, $\lambda = 0.39$ m, and $T = 0.5$ s; wave 2: $h = 0.03$ m, $\lambda = 1.56$ m, and $T = 1$ s; wave 3: $h = 0.03$ m, $\lambda = 6.25$ m, and $T = 2$ s).

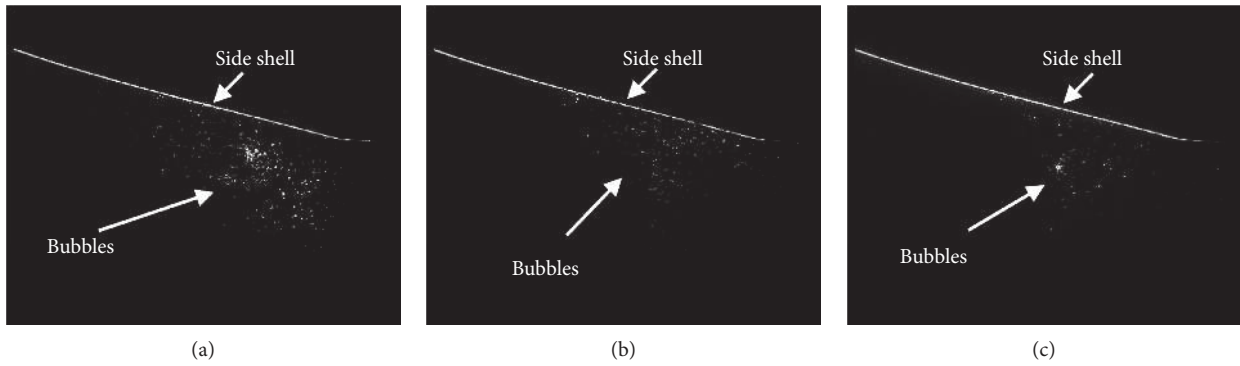


FIGURE 15: Continued.

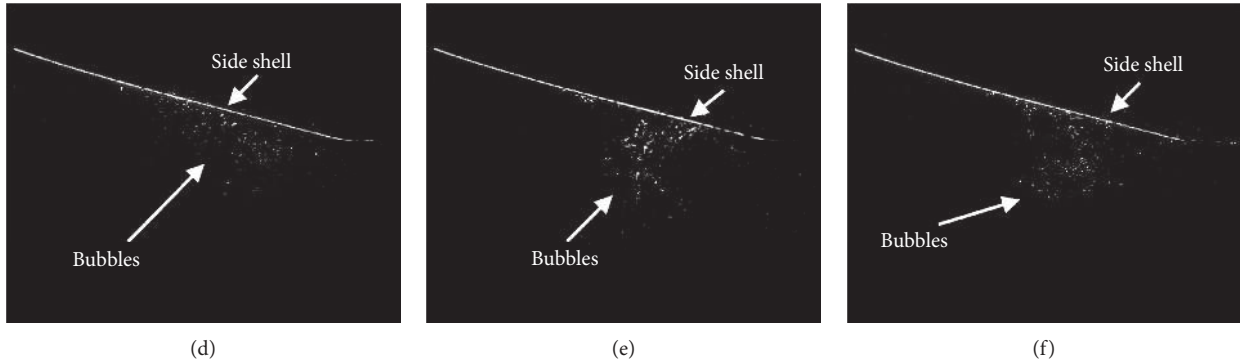


FIGURE 15: Distribution of bubbles on the transverse section at 1.07 m behind the square moonpool. (a) $t = 1.621$ s. (b) $t = 2.297$ s. (c) $t = 3.648$ s. (d) $t = 4.324$ s. (e) $t = 5.135$ s. (f) $t = 6.756$ s.

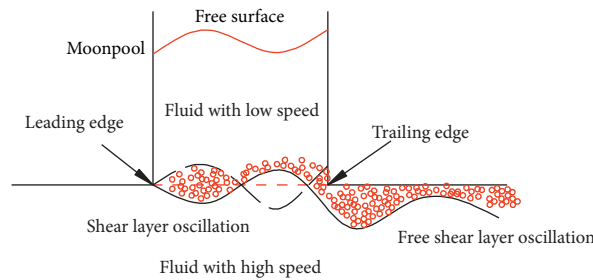


FIGURE 16: Fluid motion near the moonpool.

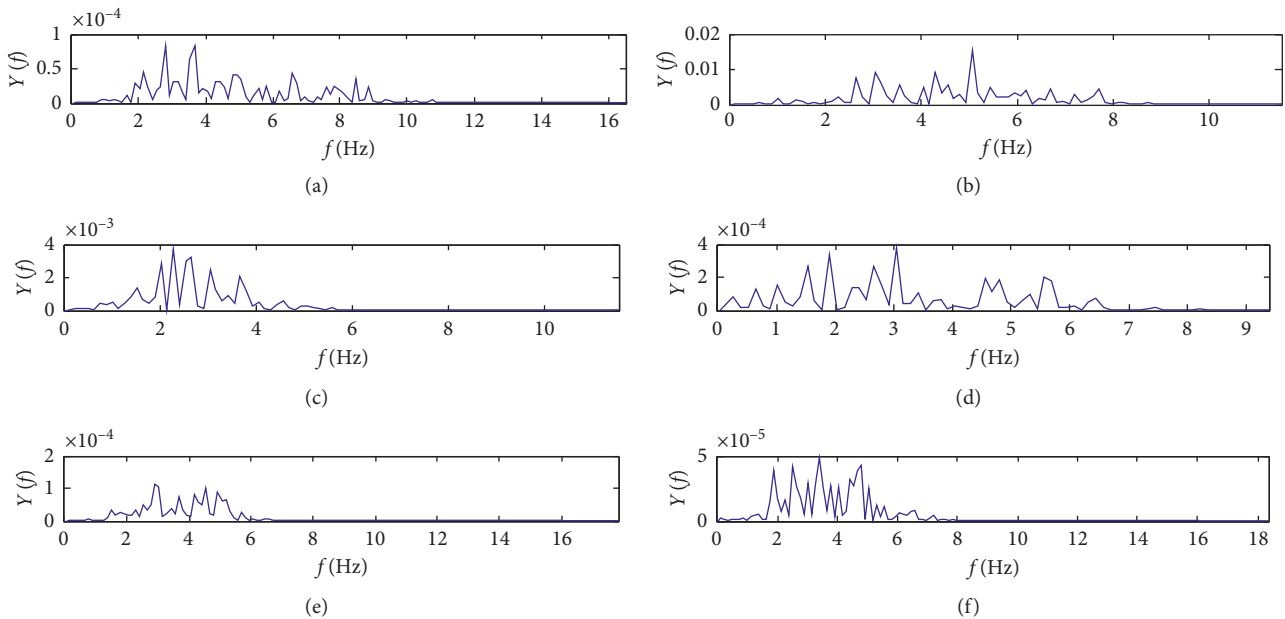


FIGURE 17: Spectrum analysis maps for the shear layer oscillation at different points along the ship bottom with $Fr = 1.83$. (a) Sensor 2. (b) Sensor 3. (c) Sensor 4. (d) Sensor 5. (e) Sensor 6. (f) Sensor 7.

It is because that when the shear layer oscillation passes from the leading edge to the trailing edge, it will impact on the trailing wall. The same frequencies of the shear layer oscillation, which are 3.036 Hz and 4.554 Hz, are found in the spectrum analysis maps for sensors 2-7. Therefore, it verifies

that the shear layer oscillation impacts on the trailing edge and detaches at the moonpool bottom to produce the free shear layer oscillation. The free shear layer oscillation flows backwards along the ship bottom in the form of the ship bottom wave.

6. Conclusion

Due to the application of the new moonpool, the detection instruments are not working properly, and the detection effect is poor. The influence of the new moonpool on the flow field around the ship must be studied. In this paper, the shear layer oscillation near the moonpool with a sonar is studied by the experimental method and the empirical mode decomposition method. The main conclusions can be summarized as follows:

- (1) Under the action of the uniform flow, the shear layer oscillation near the moonpool bottom excites the fluid motion in the moonpool.
- (2) The frequency of the shear layer oscillation near the moonpool bottom increases as the flow speed increases. The feedback of the shear layer oscillation is mainly the fluid dynamic.
- (3) Under the combined action of the wave and current, the piston motion occurs in the moonpool. The standing wave forms, which induces the sloshing motion in the moonpool.
- (4) The shear layer oscillation propagates in the form of the ship bottom wave. It affects the bubbles' distribution along the ship bottom.

Data Availability

The table and figure data used to support the findings of this study are included within the article.

Conflicts of Interest

The authors declare that they have no conflicts of interest.

Acknowledgments

The present investigation was supported and funded by the National Natural Science Foundation of China (Grant no. 51779056). All of the help is greatly appreciated and acknowledged by the authors.

References

- [1] J. Shi, F. Wen, and T. Liu, "Nested MIMO radar: coarrays, tensor modeling and angle estimation," *IEEE Transactions on Aerospace and Electronic Systems*, vol. 99, p. 1, 2020.
- [2] L. Sun, L. Wan, and X. Wang, "Learning-based resource allocation strategy for industrial IoT in UAV-enabled MEC systems," *IEEE Transactions on Industrial Informatics*, vol. 99, p. 1, 2020.
- [3] L. Wan, Y. Sun, L. Sun, Z. Ning, and J. J. P. C. Rodrigues, "Deep learning based autonomous vehicle super resolution DOA estimation for safety driving," *IEEE Transactions on Intelligent Transportation Systems*, vol. 99, pp. 1–15, 2020.
- [4] F. Wen and J. Shi, "Fast direction finding for bistatic EMVS-MIMO radar without pairing," *Signal Processing*, vol. 173, Article ID 107512, 2020.
- [5] K. Fukuda, "Behavior of water in vertical well with bottom opening of ship, and its effects on ship-motion," *Journal of the Society of Naval Architects of Japan*, vol. 1977, no. 141, pp. 107–122, 1977.
- [6] T. Kristiansen and O. M. Faltinsen, "Gap resonance analyzed by a new domain-decomposition method combining potential and viscous flow DRAFT," *Applied Ocean Research*, vol. 34, pp. 198–208, 2012.
- [7] B. Molin, "On the piston and sloshing modes in moonpools," *Journal of Fluid Mechanics*, vol. 430, pp. 27–50, 2001.
- [8] C. Gao, X. Miao, L. Lu, R. Huo, Q. Hu, and Y. Shan, "Free vibration analysis of functionally graded spherical torus structure with uniform variable thickness along axial direction," *Shock and Vibration*, vol. 2019, Article ID 2803841, 2019.
- [9] J. Gao, Z. He, J. Zang, Q. Chen, H. Ding, and G. Wang, "Topographic effects on wave resonance in the narrow gap between fixed box and vertical wall," *Ocean Engineering*, vol. 180, pp. 97–107, 2019.
- [10] T. Kristiansen and O. M. Faltinsen, "Application of a vortex tracking method to the piston-like behaviour in a semi-entrained vertical gap," *Applied Ocean Research*, vol. 30, no. 1, pp. 1–16, 2008.
- [11] S. C. Sajjan and S. Surendran, "Model tests on the moored vessel with different moonpool shapes," *Ocean Systems Engineering*, vol. 3, no. 2, pp. 137–147, 2013.
- [12] V. S. Tikhonov, V. I. Komissarenko, and B. V. Emec, "Dynamic behaviour of deepwater drilling column under collisions with drillship moonpool," *Applied Ocean Research*, vol. 13, no. 6, pp. 307–316, 1991.
- [13] H.-w. Zhou and H.-s. Zhang, "Radiation and diffraction analysis of a cylindrical body with a moon pool," *Journal of Hydrodynamics*, vol. 25, no. 2, pp. 196–204, 2013.
- [14] L.-q. Liu, H. Zhou, and Y.-g. Tang, "Coupling response of heave and moonpool water motion of a truss Spar platform in random waves," *China Ocean Engineering*, vol. 29, no. 2, pp. 169–182, 2015.
- [15] P. S. A. Michima and H. Kawabe, "Preliminary chart of drill ship operability considering moon pool sloshing effects," *Journal of Marine Science and Technology*, vol. 23, no. 1, pp. 30–41, 2018.
- [16] J. J. Park, M. S. Kim, H. S. Lee, Y. K. Ahn, Y. B. Kim, and M. K. Ha, "Development of design technologies for optimum moonpool shapes of drill ship," in *Proceedings of the ASME 2007 26th International Conference on Offshore Mechanics and Arctic Engineering*, pp. 421–426, American Society of Mechanical Engineers (ASME), San Diego, CA, USA, June 2007.
- [17] P. Sivabalan and S. Surendran, "Numerical and experimental study on varying cross-section of moonpool for a drill ship," *Ships and Offshore Structures*, vol. 12, no. 6, pp. 885–892, 2017.
- [18] S. H. Sphaier, F. G. S. Torres, I. Q. Masetti, A. P. Costa, and C. Levi, "Monocolumn behavior in waves: experimental analysis," *Ocean Engineering*, vol. 34, no. 11–12, pp. 1724–1733, 2007.
- [19] K.-M. Chung, K.-H. Lee, and K.-C. Chang, "Self-sustained oscillation for compressible cylindrical cavity flows," *Chinese Journal of Aeronautics*, vol. 30, no. 4, pp. 1294–1299, 2017.
- [20] J. Gao, J. Zang, L. Chen, Q. Chen, H. Ding, and Y. Liu, "On hydrodynamic characteristics of gap resonance between two fixed bodies in close proximity," *Ocean Engineering*, vol. 173, pp. 28–44, 2019.
- [21] A. Maurel, P. Ern, B. J. A. Zielinska, and J. E. Wesfreid, "Experimental study of self-sustained oscillations in a confined jet," *Physical Review E*, vol. 54, no. 4, p. 3643, 1996.

- [22] M. Meissner, "Self-sustained deep cavity oscillations induced by grazing flow," *Acta Acustica United with Acustica*, vol. 62, no. 3, pp. 220–228, 1987.
- [23] H. Xianghong, X. Wei, Y. Xiongliang, G. Jiayang, and J. Zhiyong, "An experimental investigation on reduction effect of damping devices for the recessing type moonpool with a large aspect ratio," *Journal of Ship Research*, pp. 1–20, 2020, In press.
- [24] W. Kang, S. B. Lee, and H. J. Sung, "Self-sustained oscillations of turbulent flows over an open cavity," *Experiments in Fluids*, vol. 45, no. 4, p. 693, 2008.
- [25] N. J. Lawson and M. R. Davidson, "Self-sustained oscillation of a submerged jet in a thin rectangular cavity," *Journal of Fluids and Structures*, vol. 15, no. 1, pp. 59–81, 2001.
- [26] S. Xiao, S. Liu, M. Song, N. Ang, and H. Zhang, "Coupling rub-impact dynamics of double translational joints with subsidence for time-varying load in a planar mechanical system," *Multibody System Dynamics*, vol. 48, no. 4, pp. 451–486, 2020.
- [27] S. Dequand, S. J. Hulshoff, and A. Hirschberg, "Self-sustained oscillations in a closed side branch system," *Journal of Sound and Vibration*, vol. 265, no. 2, pp. 359–386, 2003.
- [28] A. Seena and H. J. Sung, "Dynamic mode decomposition of turbulent cavity flows for self-sustained oscillations," *International Journal of Heat and Fluid Flow*, vol. 32, no. 6, pp. 1098–1110, 2011.
- [29] H. H. Heller and D. B. Bliss, "Flow-induced pressure fluctuations in cavities and concepts for their suppression," *Aeroacoustics: STOL Noise; Airframe and Airfoil Noise*, vol. 45, pp. 281–296, 1976.
- [30] C. W. Rowley, T. Colonius, and A. J. Basu, "On self-sustained oscillations in two-dimensional compressible flow over rectangular cavities," *Journal of Fluid Mechanics*, vol. 455, pp. 315–346, 2002.
- [31] J. Liu, J. Cai, D. Yang, J. Wu, and X. Wang, "Visualization and analysis of flow structures in an open cavity," *Modern Physics Letters B*, vol. 32, Article ID 1840010, 2018.
- [32] K. Nair and S. Sarkar, "Large eddy simulation of self-sustained cavity oscillation for subsonic and supersonic flows," *Journal of Fluids Engineering*, vol. 139, no. 1, Article ID 11102, 2017.
- [33] S. Xiao, S. Liu, H. Wang, Y. Lin, M. Song, and H. Zhang, "Nonlinear dynamics of coupling rub-impact of double translational joints with subsidence considering the flexibility of piston rod," *Nonlinear Dynamics*, vol. 100, no. 2, pp. 1203–1229, 2020.
- [34] X. Zhang, "Compressible cavity flow oscillation due to shear layer instabilities and pressure feedback," *AIAA Journal*, vol. 33, no. 8, pp. 1404–1411, 1995.
- [35] X. H. Huang, W. Xiao, X. L. Yao, J. Y. Gu, and Z. Y. Jiang, "An experimental investigation of reduction effect of damping devices in the rectangular moonpool," *Ocean Engineering*, vol. 196, Article ID 106767, 2020.